JOURNAL OF GUIDANCE, CONTROL, AND DYNAMICS
Vol. 16, No. 6, November–December 1993

Optimal Recovery from Microburst Wind Shear

Sandeep S. Mulgund* and Robert F. Stengel†
Princeton University, Princeton, New Jersey 08544

The flight path of a twin-jet transport aircraft is optimized in a microburst encounter during approach to landing. The objective is to execute an escape maneuver that maintains safe ground clearance, establishes a positive climb rate as soon as possible after the abort is triggered, and maintains an adequate stall margin during the climb out. A cost function penalizing rate of climb deviations from a nominal value and rate of elevator deflection produces qualitatively good results in a variety of microburst encounters. The optimal maneuver is a gradual pitch-up that ceases near the core of the microburst, followed by a slight reduction in pitch attitude in the tailwind area of the microburst. A minimum airspeed constraint in the optimization prevents excessive airspeed loss in very severe microbursts. The aircraft equations of motion include short-period dynamics, so that the optimization produces the control surface deflections required to achieve the optimal flight paths.

Nomenclature

D = aircraft drag
g = acceleration due to gravity
h = altitude
I_{yy} = moment of inertia about body y axis
i_T = inclination of thrust line with respect to body x axis
L = aircraft lift, cost function integrand
M = pitching moment
m = mass
q = pitch rate
R = radius of downdraft column
T = engine thrust
t = time
u = x component of aircraft velocity relative to the atmosphere
$\boldsymbol{u}$ = aircraft control vector; $[\delta_E\ \delta_T]^T$
$U_{\max}$ = maximum horizontal wind speed
V = airspeed
w = z component of aircraft velocity relative to the atmosphere
w_x = wind component along the x axis
w_z = wind component along the z axis
$\boldsymbol{w}$ = wind vector; $[w_x\ w_z]^T$
X = x component of aerodynamic and thrust forces
x = distance along x axis
$\boldsymbol{x}$ = aircraft state vector; $[x\ z\ u\ w\ q\ \theta]^T$
Z = z component of aerodynamic and thrust forces
z = distance along z axis
$z_{\max}$ = altitude of maximum outflow
α = angle of attack
δ_E = elevator deflection
δ_T = throttle setting
θ = pitch angle

Subscripts

B = measured in body coordinates
E = measured in inertial coordinates
$f, 0$ = final and initial values, respectively
x, z = measured along x and z directions, respectively

Superscript

$(\dot{})$ = time derivative

Introduction

SEVERE low-altitude wind variability represents an infrequent but significant hazard to aircraft taking off or landing. During the period from 1964 to 1985, microburst wind shear was a contributing factor in at least 26 civil aviation accidents involving nearly 500 fatalities and more than 200 injuries.[1] A microburst is a strong localized downdraft that strikes the ground, creating winds that diverge radially from the impact point.[2] An airplane penetrating the core of a microburst typically encounters an increasing wind first, which improves the apparent performance of the aircraft. When faced with the headwind, the pilot may take action to prevent the airplane from climbing. In a microburst, this headwind disappears and is quickly followed by a downdraft and tailwind, whose performance-decreasing effects may easily exceed the climb and acceleration capabilities of the airplane. Ground impact may be unavoidable if the pilot does not apply a suitable recovery technique. The physics of microbursts have only recently been understood in detail, and it has been found that effective recovery from inadvertent encounters may require piloting techniques that are counterintuitive to flight crews.[2]

The aviation community has initiated an extensive research effort to solve the wind shear problem. The Federal Aviation Administration (FAA) and NASA have established an integrated program to address the wind shear problem through focused research and development programs.[3] The objective of the program is to reduce the wind shear hazard to aircraft through the development of airborne and ground-based detection systems, crew alerting and flight management systems, and training and operating procedures.[4] The *Windshear Training Aid*[5] recommends that on recognizing an encounter with severe wind shear, the pilot should command maximum thrust and rotate the aircraft to an initial target pitch angle (TPA) of 15 deg. This pitch target was identified through rigorous analyses using full six-degree-of-freedom flight simulators and wind models representative of actual accident cases.[6] The *Windshear Training Aid* technique was developed with a number of constraints in mind. It had to be flyable by the average air-carrier pilot, easily trained in a relatively short period of time, retainable between training sessions, and generalizable to any airborne wind shear encounter (i.e., takeoff or landing). The optimal recoveries studied in this paper were not made subject to these constraints, but rather were made in the interest of exploring aircraft performance limits and identifying the qualitative nature of an optimal escape from microburst wind shear.

Presented as Paper 92-4338 at the AIAA Atmospheric Flight Mechanics Conference, Hilton Head, SC, Aug. 10–12, 1992; received Sept. 1, 1992; revision received Jan. 22, 1993; accepted for publication Jan. 23, 1993.

*Graduate Research Assistant, Department of Mechanical and Aerospace Engineering. Student Member AIAA.

†Professor, Department of Mechanical and Aerospace Engineering. Associate Fellow AIAA.

Deterministic trajectory optimization has been used to identify the limits of aircraft performance in wind shear and to determine the control strategies required to achieve such performance.[7-11] The computation of these optimal trajectories requires global knowledge of the flowfield; in other words, the wind components at all points in the aircraft's trajectory must be known in advance. Because this is not possible in practice, the results of trajectory optimization are not immediately useful for real-time control of an aircraft penetrating a wind shear. Consequently, feedback control laws have been developed that employ only local knowledge of the wind field about the aircraft for near-optimal flight control.[12-14] Most of these studies have considered the performance of jet transport (JT) aircraft in wind shear. It has been found recently that the optimal recovery technique for a commuter-class aircraft[15] is qualitatively quite different from that of a jet transport. With their relatively limited specific excess power, commuter aircraft must perform a very careful interchange between kinetic and potential energy to exit a microburst safely.

The goal of this research is to bridge the gap between the performance achieved using trajectory optimization and that attainable using feedback control based on local wind field knowledge. This paper concerns the development of optimal trajectories for a jet transport aircraft. The initial focus is on microburst encounters during approach to landing, during which the pilot makes a decision to abort an approach and to initiate a recovery maneuver.

Effect of Wind Shear on Airplane Dynamics

Aircraft Model

A six-degree-of-freedom model of a twin-jet transport aircraft is used for this study. The aircraft has a gross weight of 85,000 lb and maximum takeoff thrust of 24,000 lb. The aircraft's aerodynamic coefficients are complex, nonlinear functions of altitude, Mach number, incidence angles, rotation rates, control deflections, configuration changes (such as gear or flap deflection), and ground proximity.

Equations of Motion

This optimization study considers motion in the vertical plane only, so the lateral/directional degrees of freedom are neglected. Effects of wind shear on aircraft motion are modeled using the technique described in Ref. 16. The relevant reference frames used to describe the aircraft's position, orientation, and velocity are presented in Fig. 1. Flight is assumed to take place in a vertical plane over a flat Earth, and a coordinate system fixed to the ground is defined as the inertial frame of reference. The aircraft orientation with respect to the ground is described using the body-axis reference frame, whose origin is fixed to the aircraft's center of gravity. The airplane's airspeed is the vector sum of body-axis velocity components u and w. On the basis of these assumptions, the equations of motion are

$$\dot{x} = u\cos\theta + w\sin\theta + w_{x_E} \tag{1}$$

$$\dot{z} = -u\sin\theta + w\cos\theta + w_{z_E} \tag{2}$$

$$\dot{u} = X/m - g\sin\theta - q(w + w_{z_B}) - \dot{w}_{x_B} \tag{3}$$

$$\dot{w} = Z/m + g\cos\theta + q(u + w_{x_B}) - \dot{w}_{z_B} \tag{4}$$

$$\dot{\theta} = q \tag{5}$$

$$\dot{q} = M/I_{yy} \tag{6}$$

The force components X and Z consist of thrust and aerodynamic effects and are expressed as

$$X = T\cos i_T - D\cos\alpha + L\sin\alpha \tag{7}$$

$$Z = T\sin i_T - D\sin\alpha - L\cos\alpha \tag{8}$$

The effects of a spatially varying wind field on aircraft aerodynamics are considered in the computation of L, D, and M, as described in Refs. 16 and 17. The wind speed components are typically given in the Earth frame of reference. They must be converted to the body-axis frame for use in Eqs. (3) and (4). The relationship between wind components in these two frames of reference is

$$\begin{bmatrix} w_{x_B} \\ w_{z_B} \end{bmatrix} = \begin{bmatrix} \cos\theta & -\sin\theta \\ \sin\theta & \cos\theta \end{bmatrix} \begin{bmatrix} w_{x_E} \\ w_{z_E} \end{bmatrix} \tag{9}$$

This is expressed in vector form as

$$\boldsymbol{w}_B = \boldsymbol{L}_{BE}\boldsymbol{w}_E \tag{10}$$

The time derivatives of the wind components are required in Eqs. (3) and (4). Differentiating Eq. (10), one obtains

$$\dot{\boldsymbol{w}}_B = \dot{\boldsymbol{L}}_{BE}\boldsymbol{w}_E + \boldsymbol{L}_{BE}\dot{\boldsymbol{w}}_E \tag{11}$$

The time derivatives of the wind components in the inertial frame are

$$\begin{bmatrix} \dot{w}_x \\ \dot{w}_z \end{bmatrix}_E = \begin{bmatrix} \frac{\partial w_x}{\partial x} \\ \frac{\partial w_z}{\partial x} \end{bmatrix}_E \dot{x} + \begin{bmatrix} \frac{\partial w_x}{\partial z} \\ \frac{\partial w_z}{\partial z} \end{bmatrix}_E \dot{z} + \begin{bmatrix} \frac{\partial w_x}{\partial t} \\ \frac{\partial w_z}{\partial t} \end{bmatrix}_E \tag{12}$$

The time derivative of the transformation matrix $\boldsymbol{L}_{BE}$ is expressed as[18]

$$\dot{\boldsymbol{L}}_{BE} = -\tilde{\omega}\boldsymbol{L}_{BE} \tag{13}$$

where

$$\tilde{\omega} = \begin{bmatrix} 0 & -q \\ -q & 0 \end{bmatrix} \tag{14}$$

The wind components and spatial gradients used in the equations of motion are obtained from the Oseguera-Bowles downburst model.[19] This analytic model represents an axisymmetric stagnation point flow, based on wind velocity profiles from the Terminal Area Simulation System (TASS). The model satisfies continuity in cylindrical coordinates, and the wind components closely match real-world measurements, as

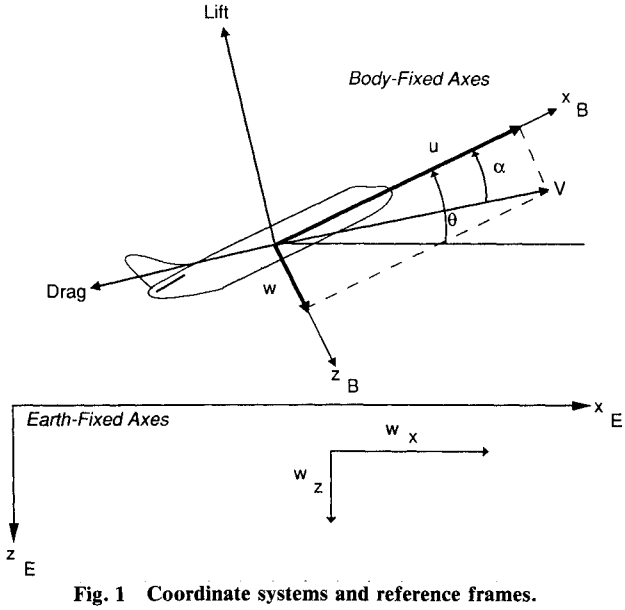

Fig. 1 Coordinate systems and reference frames.

do the increase, peak, and decay of outflow and downflow with distance from the microburst core. The objective of this work was to identify a relationship among cost function composition, microburst severity, and the shape of the resultant optimal trajectory. As such, the requirement for the microburst model was that it provide a reasonable representation of the energy losses experienced by an aircraft as it transits a microburst. Since the Oseguera-Bowles wind profiles match real-world measurements fairly well, it was considered adequate for the study. This model has been extended recently to improve its accuracy in the vortex-ring region of the microburst.[20] The flowfield is time invariant, so the partial derivatives of the wind components with respect to time in Eq. (12) are zero. Simulation of microbursts of different sizes and strengths is possible through specification of the radius of the downdraft column R, the maximum horizontal wind speed $U_{\max}$, and the altitude of maximum outflow $z_{\max}$.

Optimal Trajectories Through Wind Shear

The purpose of trajectory optimization is to determine the state and control histories $\boldsymbol{x}^*(t)$ and $\boldsymbol{u}^*(t)$ that minimize a cost function.[21] The cost function considered here consists of two parts—a scalar integral function of the state and control and a scalar algebraic function of the final state:

$$J = \phi\left[\boldsymbol{x}(t_f)\right] + \int_{t_0}^{t_f} L\left[\boldsymbol{x}(t), \boldsymbol{u}(t), \boldsymbol{w}(t), t\right] \mathrm{d}t \tag{15}$$

The choice of the Lagrangian $L[\cdot]$ and the final state penalty $\phi[\cdot]$ determines the nature of the optimizing solution. The optimal control history $\boldsymbol{u}^*(t)$ acts on the dynamic system, whose trajectory $\boldsymbol{x}^*(t)$ is determined by integrating the ordinary differential equation

$$\dot{\boldsymbol{x}} = \boldsymbol{f}\left[\boldsymbol{x}(t), \boldsymbol{u}(t), \boldsymbol{w}(t), t\right] \tag{16}$$

$$\boldsymbol{x}(t_0) = \boldsymbol{x}_0 \tag{17}$$

The dynamic system equations are those of three-degree-of-freedom aircraft motion with wind shear effects, Eqs. (1-14).

The features of the optimal trajectory through a microburst depend entirely on the chosen cost function. The objectives of the escape maneuver must be clearly identified to choose an appropriate cost function. The purpose of a recovery during approach to landing is to execute a smooth transition from descending to ascending or level flight without stalling the aircraft, saturating the controls, or impacting the ground. Transient accelerations should not exceed the structural limits of the aircraft or cause excessive passenger discomfort. Once the aircraft establishes a stable climb, it should maintain an adequate stall margin. The problem of ground avoidance can be (and has been) solved by maximizing the minimum altitude, which is a maxi-min problem of optimal control.

In principle, maximizing the minimum altitude is equivalent to minimizing the peak deviation between some high reference altitude and the aircraft's instantaneous altitude. However, the latter is a mini-max problem of optimal control. The distinction is important when developing an approximate problem that can be solved using a calculus of variations approach: The mini-max problem readily lends itself to reformulation as a Lagrangian problem of optimal control [Eq. (15)], while the maxi-min problem does not. The mini-max altitude problem was considered by Miele in his study of aborted landings in wind shear.[22] The cost function is

$$\min I = \max_t \left[h_{\mathrm{ref}} - h(t)\right] \qquad t_0 \le t \le t_f \tag{18}$$

This is a Chebyshev problem of optimal control, which can be reformulated as a Lagrangian problem of optimal control where one minimizes the integral cost function

$$J = \int_{t_0}^{t_f} \left[h_{\mathrm{ref}} - h(t)\right]^p \mathrm{d}t \tag{19}$$

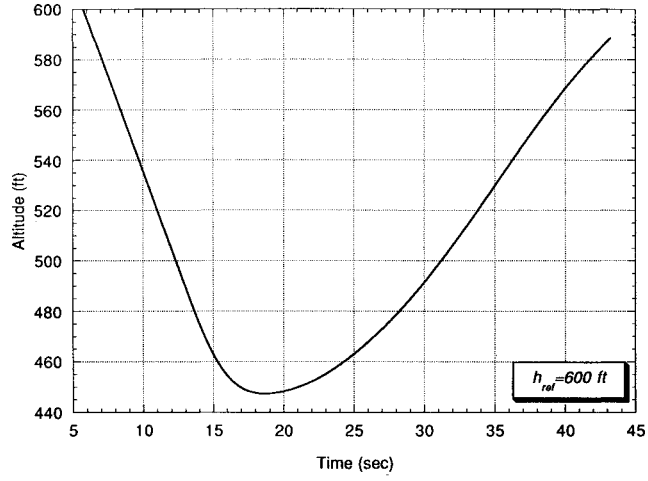

Fig. 2 Altitude vs time for a typical trajectory.

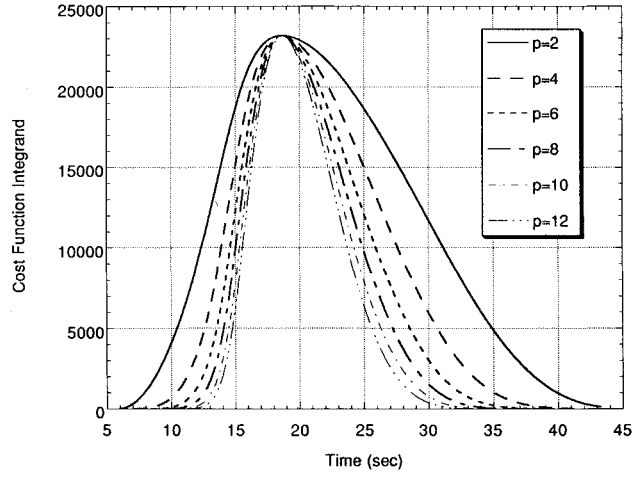

Fig. 3 Altitude cost function integrands for varying values of p.

and p is a large, even, positive integer. As p is increased, the peak of the function dominates the area under the curve. Figures 2 and 3 illustrate the idea. A typical altitude time history is presented in Fig. 2, and a set of corresponding cost function integrands is illustrated in Fig. 3. Each of the curves in Fig. 3 represents a function of the form

$$L[\boldsymbol{x}(t)] = [h_{\mathrm{ref}} - h(t)]^p \tag{20}$$

for varying even values of p. The functions have been scaled so that their peaks all have the same magnitude. The peak of the integrand represents the maximum difference between h_{ref} and $h(t)$. As p increases, the area underneath the integrand function is increasingly dominated by the height of the peak. Thus as p is increased, Eq. (19) becomes a better and better approximation for the problem defined by Eq. (18). Typically, p values of 6 or 8 provide a reasonable solution. A drawback of an excessively large value of p is that the Euler-Lagrange equations[21] used to compute the optimal solution become more difficult to solve. The choice of the constant h_{ref} also affects the solution. Thus although the maxi-min cost function represents an absolute maximization of the minimum altitude, the integral equivalent mini-max cost function does not.

The optimal solution to Eq. (19) shapes the aircraft trajectory in such a way that the maximum difference between h_{ref} and $h(t)$ is minimized, given the performance limits of the aircraft and the severity of the wind shear. Although it is effective at this task, it provides little control over the trajectory after the point of minimum altitude, other than causing the aircraft to climb. Once the aircraft establishes a positive

rate of climb, it is desirable to regulate airspeed and/or rate of climb. This could have been accomplished by including additional terms in the cost function, but a different approach was taken. Difficulty in integrating the Euler-Lagrange equations here and in an earlier commuter-aircraft study[15] motivated the use of a quadratic cost function, which is easier to optimize than a cost function containing larger exponents and produces similar (but not identical) results. Because rate of climb was of interest, it was used directly in the cost function. The Lagrangian had the general form

$$L\left[\boldsymbol{x}(t),\, \boldsymbol{u}(t)\right] = k_{\dot{h}}\left[\dot{h}(t) - \dot{h}_{\text{ref}}\right]^2 + k_q q(t)^2 + k_{\delta_E}\delta_E(t)^2 + \dot{k}_{\dot{\delta}_E}\dot{\delta}_E(t) \tag{21}$$

The first term penalizes deviations from a nominal target rate of climb $\dot{h}_{\text{ref}}$, whereas the remaining terms penalize pitch rate, elevator deflection, and rate of elevator deflection, respectively. The last three terms are added to introduce different means of controlling the transient motion from descending to ascending flight. The scalar in front of each term weights its relative contribution to the cost function. In its basic form (i.e., without the last three terms), the altitude rate cost function penalizes any deviations from the target climb rate. Because the aircraft begins the recovery in a state of descent, the optimization algorithm applies control inputs immediately to make as rapid a transition as possible to an ascent at the target climb rate. In a sense, this is equivalent to minimizing the altitude drop of the aircraft. When the additional terms are put into the cost function, the climb rate objective becomes weighted against the objective of minimizing pitch rate, elevator deflection, or elevator rate.

Table 1 Cost function weights for optimization

Trajectory	$k_{\dot{h}}$, ft/s	k_q, s	k_{δ_E}, deg	$k_{\dot{\delta}_E}$, deg/s
1	0.1	0.0	0.0	0.0
2	0.1	3.0	0.0	0.0
3	0.1	0.0	0.5	0.0
4	0.1	0.0	0.0	5.0

Several optimal trajectories were computed for microburst encounters during a final approach. Optimal trajectories were first computed using different sets of values for k_q, k_{δ_E}, and $k_{\dot{\delta}_E}$ to determine the impact of these terms on the qualitative nature of the escape maneuver. Another set of optimal trajectories was then computed, using a fixed set of weights and microbursts of varying intensity, to assess the effect of shear strength on the optimal flight paths.

Effect of Cost Function on Optimal Flight Paths

Optimal trajectories were calculated for microburst encounters during approach to landing. The Lagrangian was defined

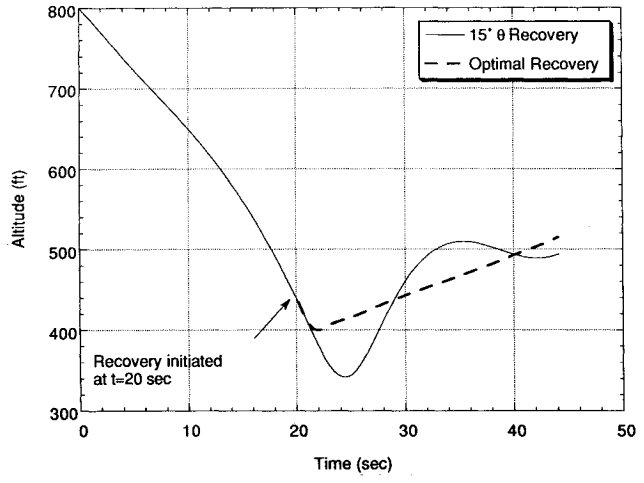

Fig. 4 Altitude vs time for the nominal and optimal recoveries.

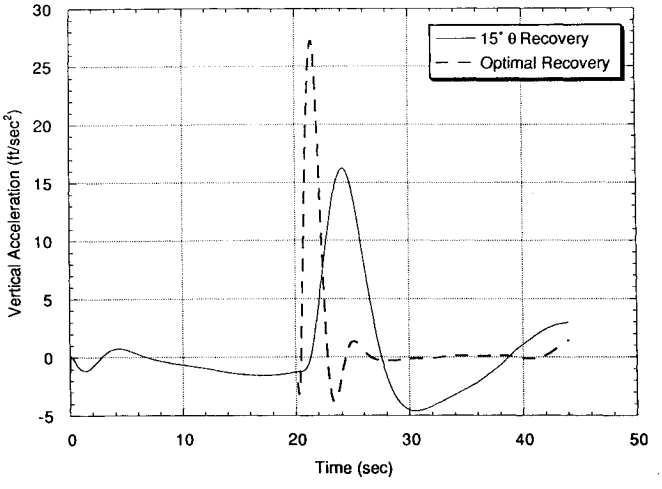

Fig. 5 Vertical acceleration vs time for the nominal and optimal recoveries.

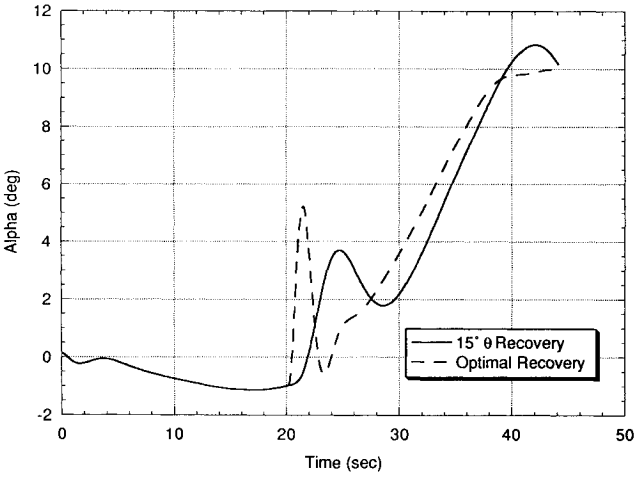

Fig. 6 Angle of attack vs time for the nominal and optimal recoveries.

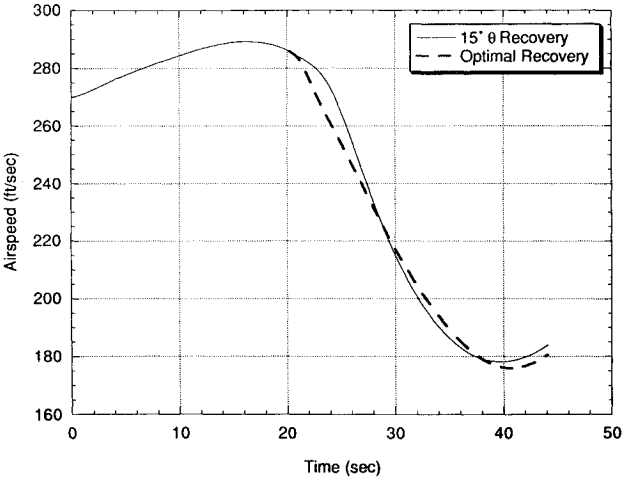

Fig. 7 Airspeed vs time for the nominal and optimal recoveries.

by Eq. (21), and a conjugate gradient method[23] was used to minimize Eq. (15). The nominal state and control histories used to initiate the optimization were those of a recovery performed using the 15-deg θ technique. The recovery was initiated the instant that the aircraft was within a distance R of the microburst core, where R is the radius of the downdraft column. Range from core was used to trigger the recoveries to identify the effect of microburst severity on the shape of the optimal flight paths when the aircraft initiates the maneuver with consistent initial conditions in all cases. As a practical matter, it should be noted that range from core probably will not be known in a real microburst encounter. More likely, a recovery will be triggered by a reactive detection system that estimates air mass acceleration by differencing inertial acceleration signals from air mass-derived quantities.

The microburst had a core radius of 3000 ft, a maximum horizontal wind speed of 80 ft/s, and an altitude of maximum outflow of 150 ft. The aircraft was initialized on a final approach 7000 ft from the microburst core at an altitude of 800 ft. Flaps were fixed at the approach setting of 30 deg. Table 1 summarizes the weights used in each of the optimal trajectories. In all cases, the target rate of climb $\dot{h}_{\text{ref}}$ was set at 300 ft/min. Maximum thrust was commanded as soon as the recovery was initiated. The engine spool-up delay was simulated using a 2-s first-order lag.

Figure 4 presents altitude vs time for the nominal 15-deg θ recovery and optimal trajectory 1, which had the highest minimum altitude. Figure 5 presents vertical acceleration vs time for both trajectories, and Fig. 6 presents angle of attack vs time for both trajectories. The vertical acceleration is defined as the second derivative of altitude with respect to time, $\ddot{h}(t)$. The airspeed histories for both trajectories are shown in Fig. 7. The airspeed increased until about $t = 16$ s, indicating that the aircraft experienced a performance-increasing shear for the first 16 s of the encounter. Beyond $t = 16$ s, the airspeed started to decrease, and the recovery was initiated 4 s later. The vertical acceleration transient very early in the trajectory was caused by a slight trim error in the aircraft's initial conditions. The subsequent negative acceleration (i.e., toward the ground) was caused by the aircraft's entry into the downdraft region of the microburst. The maximum vertical acceleration the aircraft experienced during the nominal recovery was about 0.5 g. This suggests that a higher minimum altitude could have been achieved in the 15-deg θ recovery with more aggressive control deflections. It was found that tightening the gain from pitch angle to elevator angle resulted in a higher minimum altitude, at the expense of a much smaller stall margin (and higher angles of attack) later in the microburst encounter. Since the 15-deg θ recovery was performed only to provide a starting point for the optimization, a refined pitch-attitude controller including stall prevention logic was not developed.

Optimal trajectory 1 had a minimum altitude approximately 55 ft higher than that of the nominal recovery. Although this trajectory might represent the best altitude performance achievable in theory, it is not a realistic flight path. In the first few seconds of the maneuver, the aircraft experiences pitch rates of 15 deg/s and elevator rates of 50 deg/s. Conventional JT actuators typically cannot achieve so high an elevator rate. It is evident that the optimal recovery is a very aggressive maneuver from the various state histories. There is a sharp increase in angle of attack early in the recovery, and it peaks at about 10 deg at the end of the encounter. The stall angle of attack of the aircraft is approximately 16 deg. The maximum vertical acceleration of the aircraft is nearly 1 g. The remaining three optimal trajectories were computed to achieve a more reasonable transient maneuver from descending to ascending flight. Altitude time histories are presented for all four optimal trajectories in Fig. 8, pitch attitude histories are in Fig. 9, and elevator angle histories are shown in Fig. 10. Finally, vertical acceleration histories are presented in Fig. 11. It is clear from this figure that adding the various additional terms had a pronounced effect on the aircraft's transient acceleration.

The choice of the Lagrangian has a substantial effect on each of the flight paths. The optimal maneuver is not a pitch-up toward some constant target attitude but a gradual increase in pitch attitude that ceases just past the core of the microburst. In the tailwind area of the microburst, the pitch attitude is reduced slightly. Trajectories 2–4 evince relatively smooth transitions from descending to ascending flight, but they are somewhat different from one another. In trajectory 2, the aircraft does not pitch up as rapidly as in trajectory 1, but the initial motion of the elevator is very rapid. During the climb-out portion of the trajectory, the aircraft does achieve the desired climb rate. In trajectory 3, the initial elevator motion is fairly rapid, although not as severe as that of trajectory 1. However, in this case the aircraft does not quite achieve the desired climb rate of 300 ft/min. During the climb-out portion of the trajectory, the optimization algorithm trades off climb rate for elevator usage to minimize the cost function as much as possible. Transient elevator motion in the first few seconds is reduced, but the fact that the aircraft does not achieve the desired climb rate renders this trajectory undesirable. This limitation is overcome in trajectory 4, where the cost function penalized the elevator rate directly, producing very gradual motions in the elevator angle. During the climb out, the aircraft did achieve the desired climb rate of 300 ft/min. The aircraft could achieve a higher minimum altitude by reducing the relative weighting of elevator rate in the cost function.

An important property of these optimal trajectories is their flyability. Trajectories that require very complicated control actions may not be flyable in practice if the required guidance

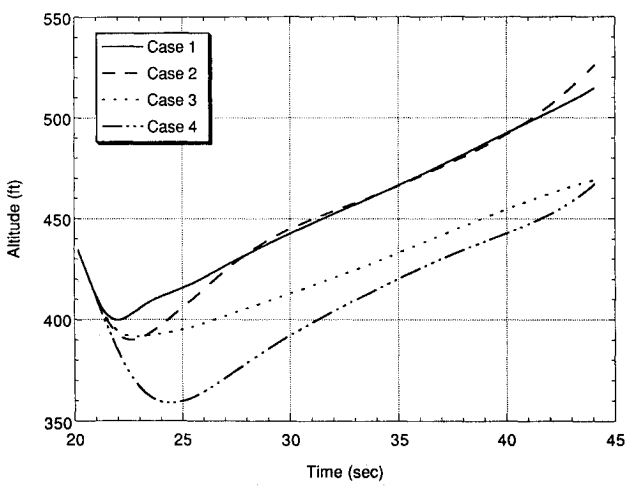

Fig. 8 Altitude vs time for optimal trajectories using four different cost functions.

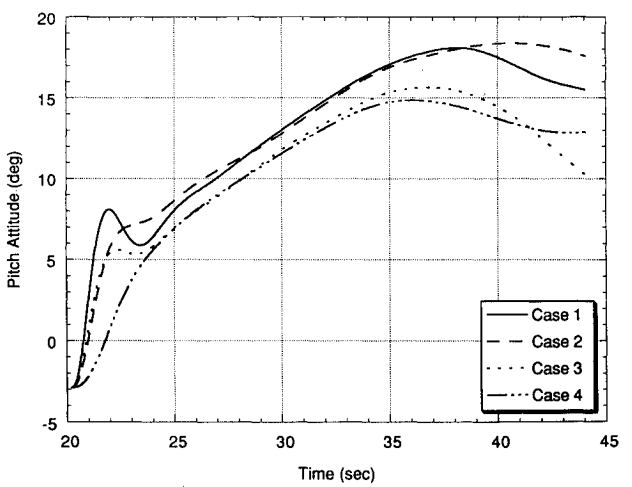

Fig. 9 Pitch attitude vs time for optimal trajectories using four different cost functions.

logic is being used as the basis of flight-director commands to the pilot. From Fig. 9, it is apparent that all trajectories are gradual increases in pitch attitude that cease just past the microburst core. There is a slight reduction in pitch attitude in the tailwind region of each of the microbursts. Figure 10 shows that the elevator action is relatively uncomplicated; the stick is pulled back to begin the recovery and then gradually let forward as the event progresses. The monotonic changes in pitch attitude and elevator angle through most of the recovery suggest that these optimal trajectories represent reasonable maneuvers.

Trajectories 2–4 present different techniques for controlling the transition from descending to ascending flight. As discussed earlier, this transition should be performed without saturating the controls or producing excessive vertical acceleration. The cost function could include an acceleration term directly, because it is a variable that is of interest, but vertical acceleration is a relatively complicated function of the aircraft state. As a practical matter, cost functions that are relatively simple functions of the aircraft state are easier to optimize than ones that contain complicated nonlinear functions. Because the elevator rate term in the cost function indirectly reduced the magnitude of the acceleration transient, it was used to expedite the optimization process.

Effect of Microburst Severity on Optimal Flight Paths

The effect of microburst severity on the nature of optimal recoveries is now explored. Optimal flight paths were computed through microbursts of varying peak horizontal wind speed to ascertain the effect of microburst severity on the shape of the optimal flight paths. Table 2 presents the parameter sets used with the Oseguera-Bowles model.[19]

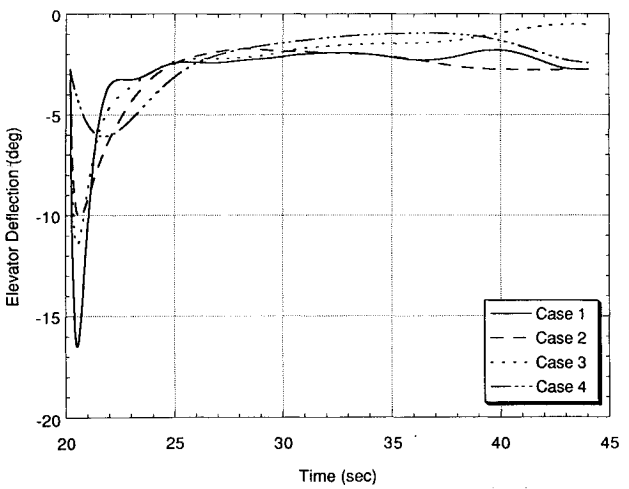

Fig. 10 Elevator deflection vs time for optimal trajectories using four different cost functions.

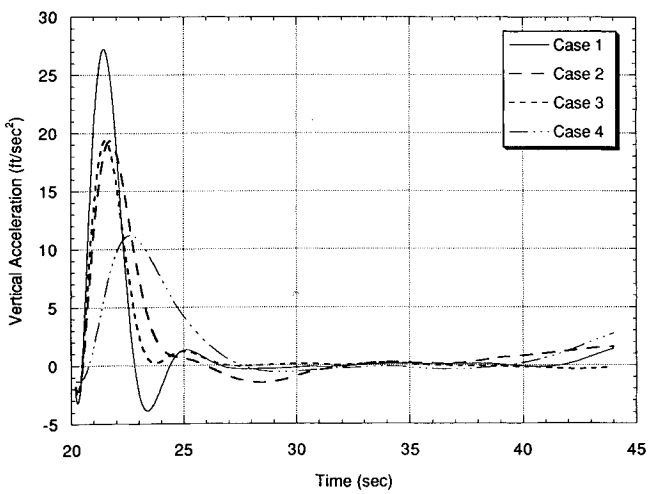

Fig. 11 Vertical acceleration vs time for optimal trajectories using four different cost functions.

Table 2 Parameter sets for investigation of effect of microburst severity

Microburst no.	R, ft	U_{max}, ft/s	z_{max}, ft
1	3000	60	150
2	3000	70	150
3	3000	75	150
4	3000	80	150

Table 3 Cost function weights for second optimization example

Weight	Value
$k_{\dot{h}}$	0.1 ft/s
$k_{\dot{\delta}}$	1.0 deg/s
k_V	0.1 ft/s

A minimum airspeed constraint was added to the cost function to prevent the aircraft from coming too close to its stall speed (about 100 Kt in the approach configuration). The cost function was modified so that it would attempt to maintain a 25-Kt airspeed buffer above the stall speed. The Lagrangian used was

$$L(\boldsymbol{x}, \boldsymbol{u}) = k_{\dot{h}}\left[\dot{h}(t) - \dot{h}_{\text{ref}}\right]^2 + k_{\dot{\delta}_E}\dot{\delta}_E(t)^2 + L_V\left[V(t)\right] \tag{22}$$

The incremental cost function L_V was added as a soft constraint to prevent excessive violation of the airspeed constraint. This function remains zero provided that its argument does not violate a predefined limit. Once the limit is violated, its contribution to the Lagrangian grows quadratically with the magnitude of the violation. Thus,

$$L_V\left[V(t)\right] = \begin{cases} k_V\left[V(t) - V_{\min}\right]^2 & V \le V_{\min} \\ 0 & V > V_{\min} \end{cases} \tag{23}$$

The parameter $V_{\min}$ was set at 125 Kt. The degree to which the aircraft violates the airspeed constraint depends on the relative magnitude of k_V and the other weights in the Lagrangian. Table 3 presents the cost function weights used for the generation of these optimal flight paths. The elevator rate weighting was reduced slightly from the previous example to achieve a higher minimum altitude. By reducing the relative weight of the elevator rate term, the cost function was biased more toward the climb rate tracking objective. The scaling on elevator rate was reduced enough to realize a significant increase in minimum altitude without generating unrealistic elevator rates.

Each of the flight paths was optimized using the same technique described earlier. The aircraft was initialized on the glide slope just outside the core region, and the recovery was initiated once the core was penetrated. Figure 12 presents altitude vs range from core for each of the microburst encounters. The corresponding airspeed histories are shown in Fig. 13, and Fig. 14 presents the climb rate histories. Figure 15 presents angle of attack vs range for each of the trajectories.

All four optimal flight paths were transitions from descending to ascending flight. However, the introduction of the minimum airspeed penalty function had a significant effect on the aircraft's climb rate during the escape. In the two weakest microbursts, the aircraft was able to maintain the reference climb rate of 5 ft/s (300 ft/min) without violating the penalty function threshold. In the two strongest microbursts, the aircraft did not reach a climb rate of 5 ft/s until the encounter was almost over. Figure 13 reveals that the airspeed did violate

the penalty function threshold somewhat in these encounters. If the airspeed constraint had not been present in these microbursts, the aircraft would likely have reached the 5-ft/s climb rate early in the encounter and come close to stall later in the event. As seen in Fig. 14, the introduction of the penalty function caused the optimization algorithm to settle on a reduced climb rate through most of the microburst to prevent excessive violation of the penalty function threshold later on. The degree to which the airspeed drops below 125 Kt could be altered by changing the relative magnitude of the climb rate and airspeed weights in the cost function [Eq. (18)]. From Fig. 15, it can be seen that the maximum angle of attack experienced by the aircraft in microburst 4 is much lower than in trajectory 1 (which used the same microburst parameters) of the first optimization example presented earlier in this paper. The transient increase in angle of attack early in the recovery is also much smaller than in trajectory 1, in which elevator rate was not a component of the cost function. The airspeed penalty function had the indirect effect of reducing the peak angle of attack during the recovery maneuver. Although it was not necessary in this study, another penalty function could be added to the cost function to limit the angle of attack to less than some maximum permissible value. This could have been an issue had the wind model contained updrafts associated with vortex rings. Such updrafts could result in transient increases in α without a corresponding airspeed loss.

Microburst severity has thus been found to have a significant effect on the nature of an optimal recovery using the given cost function. In weak-to-moderate microbursts, the aircraft easily tracks the reference climb rate throughout the encounter. However, in a severe microburst the aircraft settles on a reduced climb rate through much of the encounter to prevent excessive airspeed loss. Although these results are useful for providing insight into the nature of optimal recovery techniques, they are not immediately useful for real-time feedback control. Global knowledge of the flowfield is required for optimization. Even with the advent of forward-look sensors,[3] such detailed information about a microbursts structure will not be available. Furthermore, optimization is itself an iterative, time-consuming process.

Current work involves development of nonlinear inverse-dynamic control laws for airspeed/groundspeed and flight-path tracking in wind shear. Future work will involve the use of forward-looking sensors for estimating the anticipated energy loss in a microburst. It should be possible to use such information for near-optimal flight guidance in wind shear. An estimate of microburst-induced energy loss would be more useful as a basis for initiating an aborted landing than an instantaneous measurement of shear intensity. As pointed out by Bowles,[3] it is microburst intensity and spatial extent that determine the hazard level posed to an aircraft. The insight gained from this optimization study could be used to guide a maneu-

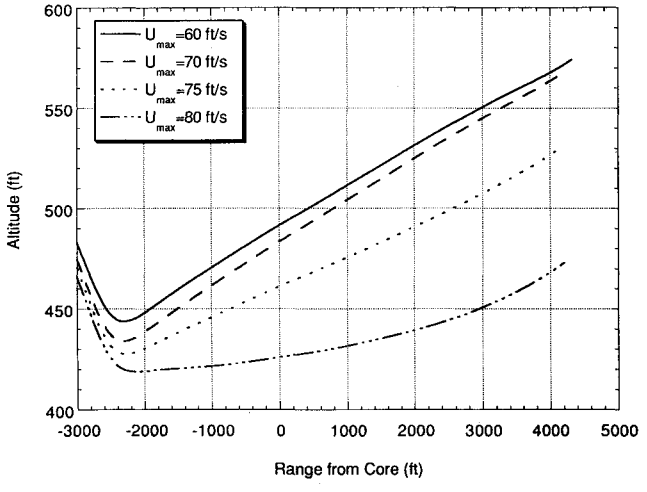

Fig. 12 Altitude vs range from core in four different microbursts.

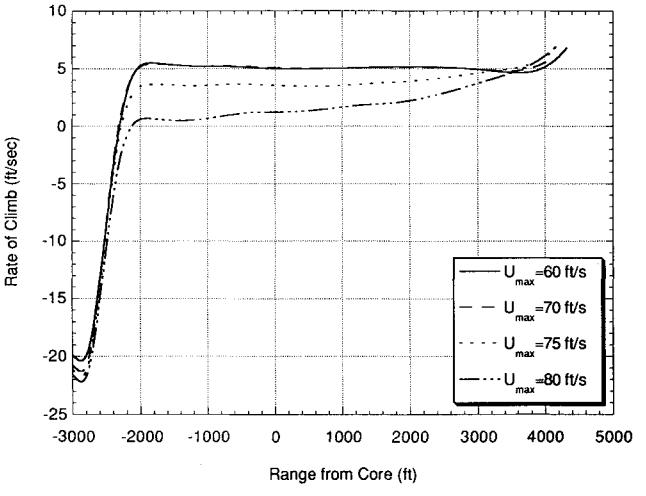

Fig. 14 Rate of climb vs range from core in four different microbursts.

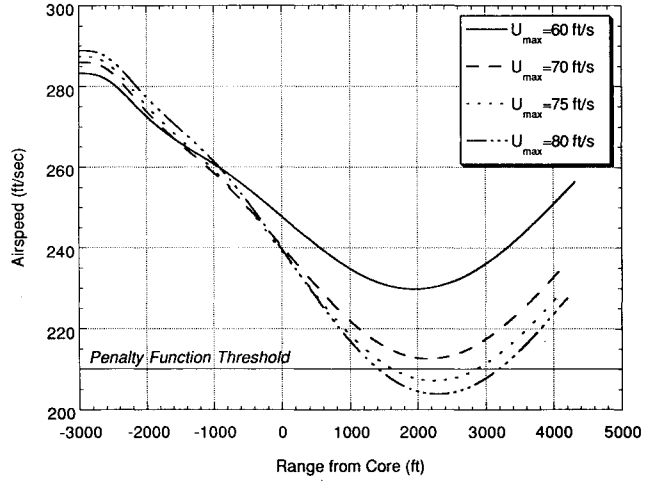

Fig. 13 Airspeed vs range from core in four different microbursts.

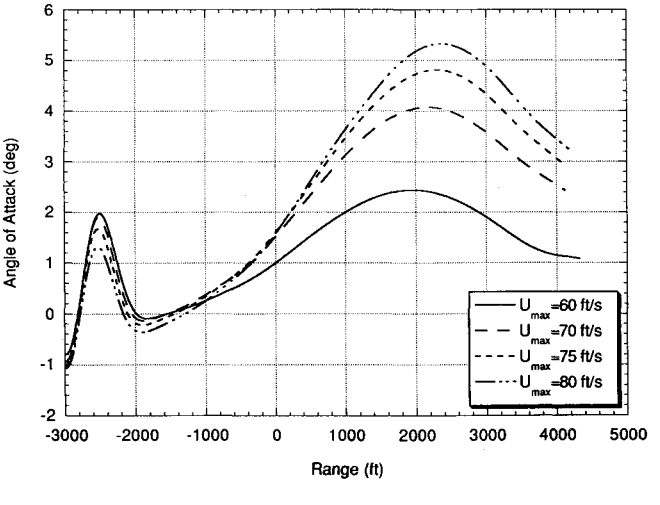

Fig. 15 Angle of attack vs range from core in four different microbursts.

ver from descending to ascending flight when a recovery is considered necessary. It will be necessary to parameterize the relationship between microburst severity, aircraft energy state, and the shape of the optimal flight path to make this possible. Significant estimation issues exist as well. In particular, forward-looking Doppler sensors are capable of measuring wind components along the line-of-sight only; vertical wind content can only be inferred from the measured radial winds and perhaps ground-based measurements.

Conclusions

The results of this optimization study have shown that there is a material relationship between cost function composition, microburst severity, and the shape of an optimal flight path through microburst wind shear. The specific cost function chosen for an optimization problem has a significant effect on the qualitative features of the solution. The goal of flight-path tracking during a recovery maneuver was achieved using a cost function penalizing deviations in climb rate from a target value. Different means of regulating the transition from descending to ascending flight were explored. It was found that penalizing rate of elevator deflection produced the most acceptable recoveries from microburst wind shear during approach to landing. A minimum airspeed constraint was incorporated in the optimization using a penalty function method.

Microburst severity has a pronounced effect on the shape of the optimal flight paths with the chosen cost function. In weak microbursts, the aircraft was able to track a reference climb rate throughout most of the encounter. In very severe microbursts, however, the aircraft settled on a reduced climb rate early in the encounter to prevent excessive airspeed loss. Future work will address the formulation of real-time guidance and control laws that approximate the performance realized in the optimal flight paths.

Acknowledgments

This research has been sponsored by the FAA and the NASA Langley Research Center under Grant NGL 31-001-252.

References

[1]Townsend, J., *Low-Altitude Wind Shear and Its Hazard to Aviation*, National Academy Press, Washington, DC, 1983.

[2]Hinton, D. A., "Flight Management Strategies for Escape From Microburst Encounters," NASA TM 4057, 1988.

[3]Bowles, R. L., "Reducing Windshear Risk Through Airborne Systems Technology," 17th Congress of the International Council of the Aeronautical Sciences, Stockholm, Sweden, 1990.

[4]Hinton, D. A., "Piloted-Simulation Evaluation of Recovery Guidance for Microburst Wind Shear Encounters," NASA TP 2886, 1989.

[5]*Windshear Training Aid*, U.S. Department of Transportation, Federal Aviation Administration, Washington, DC, 1987.

[6]Kupcis, E. A., "Manually Flown Windshear Recovery Technique," *Proceedings of the 29th Conference on Decision and Control*, Honolulu, HI, Dec. 1990, pp. 758–759.

[7]Miele, A., "Optimal Trajectories and Guidance Trajectories for Aircraft Flight Through Windshears, *Proceedings of the 29th Conference on Decision and Control*, Honolulu, HI, Dec. 1990, pp. 737–746.

[8]Psiaki, M. L., and Stengel, R. F., "Analysis of Aircraft Control Strategies for Microburst Encounter," *Journal of Guidance, Control, and Dynamics*, Vol. 8, No. 5, 1985, pp. 553–559.

[9]Psiaki, M. L., "Control of Flight Through Microburst Wind Shear Using Deterministic Trajectory Optimization," Ph.D. Dissertation, Princeton Univ., Princeton, NJ, Rept. 1787-T, 1987.

[10]Psiaki, M. L., and Stengel, R. F., "Optimal Aircraft Performance During Microburst Encounter," *Journal of Guidance, Control, and Dynamics*, Vol. 14, No. 2, 1991, pp. 440–446.

[11]Zhao, Y., and Bryson, A. E., Jr., "Optimal Paths Through Downbursts," *Journal of Guidance, Control, and Dynamics*, Vol. 13, No. 5, 1990, pp. 813–818.

[12]Zhao, Y., and Bryson, A. E., Jr., "Control of an Aircraft in Downbursts," *Journal of Guidance, Control, and Dynamics*, Vol. 13, No. 5, 1990, p. 819.

[13]Miele, A., Wang, T., and Melvin, W. W., "Guidance Strategies for Near-Optimum Takeoff Performance in Wind Shear," *Journal of Optimization Theory and Applications*, Vol. 50, No. 1, July 1986.

[14]Miele, A., Wang, T., and Melvin, W., "Optimization and Gamma/Theta Guidance of Flight Trajectories in a Windshear," 15th ICAS Congress, London, Sept. 1986.

[15]Mulgund, S. S., and Stengel, R. F., "Target Pitch Angle for the Microburst Escape Maneuver," 30th Aerospace Sciences Meeting, AIAA Paper 92-0730, Reno, NV, Jan. 1992; also *Journal of Aircraft* (to be published).

[16]Frost, W., and Bowles, R. L., "Wind Shear Terms in the Equations of Aircraft Motion," *Journal of Aircraft*, Vol. 21, No. 11, 1984, pp. 866–872.

[17]Stengel, R. F., *Course Notes for MAE 566: Aircraft Dynamics*, Princeton Univ., Princeton, NJ, Jan. 1990.

[18]Etkin, B., *Dynamics of Atmospheric Flight*, Wiley, New York, 1972.

[19]Oseguera, R. M., and Bowles, R. L., "A Simple, Analytic Three-Dimensional Downburst Model based on Boundary Layer Stagnation Flow," NASA TM 100632, 1988.

[20]Vicroy, D. D., "A Simple, Analytical, Axisymmetric Microburst Model for Downdraft Estimation," NASA TM 104053, Feb. 1991.

[21]Stengel, R. F., *Stochastic Optimal Control: Theory and Application*, Wiley-Interscience, New York, 1986.

[22]Miele, A., Wang, T., Tzeng, C. Y., and Melvin, W. W., "Optimization and Guidance of Abort Landing Trajectories in a Windshear," *Proceedings of the AIAA Guidance, Navigation, and Control Conference* (Monterey, CA), AIAA, Washington, DC, 1987, pp. 483–509.

[23]Lasdon, L. S., Mitter, S. K., and Waren, A. D., "The Conjugate Gradient Method for Optimal Control Problems," *IEEE Transactions on Automatic Control*, Vol. AC-12, No. 2, 1967.